Analysis of spanning avalanches in the two-dimensional nonequilibrium zero-temperature random-field Ising model

Djordje Spasojević, Sanja Janićević, and Milan Knežević
University of Belgrade, Faculty of Physics, POB 44, 11001 Belgrade, Serbia
(Received 4 September 2013; published 15 January 2014)

We present a numerical analysis of spanning avalanches in a two-dimensional (2D) nonequilibrium zero-temperature random field Ising model. Finite-size scaling analysis, performed for distribution of the average number of spanning avalanches per single run, spanning avalanche size distribution, average size of spanning avalanche, and contribution of spanning avalanches to magnetization jump, is augmented by analysis of spanning field (i.e., field triggering spanning avalanche), which enabled us to collapse averaged magnetization curves below critical disorder. Our study, based on extensive simulations of sufficiently large systems, reveals the dominant role of subcritical 2D-spanning avalanches in model behavior below and at the critical disorder. Other types of avalanches influence finite systems, but their contribution for large systems remains small or vanish.

DOI: 10.1103/PhysRevE.89.012118 PACS number(s): 64.60.Ht, 75.60.Ej, 75.40.Mg, 75.50.Lk

I. INTRODUCTION

Over the past few decades, the study of nonequilibrium systems, manifesting avalanche-type response in relaxation to external perturbation, played an important role. Thus, in the research of disorder-induced phase transitions, a particular focus was on the random field Ising model (RFIM) [1] and its nonequilibrium zero-temperature version [2,3], due to their conceptual importance and relevance for interpretation of Barkhausen noise data [4–6].

Extensive studies on nonequilibrium zero-temperature RFIM revealed its nontrivial critical behavior in $2 \leqslant d < 6$ dimensions and the mean-field criticality for $d \geqslant 6$ [7–12]. In addition, it has been shown that both equilibrium [13] and nonequilibrium zero-temperature models are very likely to be in the same universality class for $d \geqslant 3$ [14]. On the other hand, the two models are different in the two-dimensional (2D) case because the ferromagnetic ordering, found in the nonequilibrium 2D model [11,12], is absent in the thermodynamic limit of the equilibrium 2D model [15].

A significant part of recent studies of nonequilibrium systems are concentrated on extreme events, comprising catastrophic runaway avalanches in which a majority of the system's constituents change their state [16,17]. Extreme statistics of avalanches near the depinning transition have been also studied in Refs. [18,19], leading to results that are broadly applicable to other systems, ranging from magnets to crystal plasticity [20]. Beside physics, the analysis of extreme events is widely used in other sciences, such as technical, material, earth, and climate sciences, as well as for predictions related to finance and traffic systems. Many of these systems can be treated as nonequilibrium and 2D, which was an additional motive of this study of a nonequilibrium 2D model.

A decade ago, Pérez-Reche and Vives introduced an extensive finite-size scaling analysis of spanning avalanches in the three-dimensional (3D) model [21]. They have identified the type of spanning avalanches that survive the thermodynamical limit below critical disorder and found that other types of spanning avalanches are irrelevant in this limit except at critical disorder.

During a single simulation of 3D and higher dimensional models, more than one spanning avalanche may be triggered. This is not the case in the 2D model where at most one spanning avalanche per run may appear, which necessitates a modification of the foregoing analysis.

In this paper we present a numerical study of the spanning avalanches in the 2D nonequilibrium zero-temperature random-field Ising model. In addition to finite-size scaling analysis of various spanning avalanche distributions, we introduce an analysis of a *spanning field*, i.e., a field that triggers a spanning avalanche, which enabled us to perform the collapsing of averaged magnetization curves below critical disorder.

Our paper is organized as follows. In Sec. II we briefly describe the random field Ising model, and in Sec. III we outline the role of spanning avalanches for the RFIM critical behavior. Classification of spanning avalanches in 2D model, together with numerical analysis of their average number, and of their fractal properties, are given in Sec. IV. Scaling analyses of spanning avalanche size distribution and of magnetization jumps, presented in Secs. V and VI, are followed by a scaling analysis of spanning fields in Sec. VII and a scaling analysis of averaged magnetization curves below critical disorder in Sec. VIII. Our findings are discussed in Sec. IX and summarized in Sec. X.

II. MODEL

The random field Ising model (RFIM) describes a system of N ferromagnetically coupled spins $S_i = \pm 1$ located at sites i of a d-dimensional Euclidean lattice, here the quadratic lattice ($d = 2$) of size $L \times L$ with periodic boundary conditions. In its simplest form, the Hamiltonian of this system is

$$\mathcal{H} = -\sum_{\langle i,j \rangle} S_i S_j - H \sum_i S_i - \sum_i h_i S_i, \qquad (1)$$

where $\langle i,j \rangle$ are the pairs of nearest neighbors, H is a homogeneous external magnetic field, while $\{h_i\}_{i=1}^N$ is some configuration of the local quenched magnetic field. Its values h_i at $N = L^2$ lattice sites are randomly chosen from some zero-mean distribution, here Gaussian distribution

$$\rho(h) = \frac{1}{R\sqrt{2\pi}} \exp\left(-\frac{h^2}{2R^2}\right) \qquad (2)$$

with standard deviation R, controlling disorder in the system. The values of random variables $\{h_i\}_{i=1}^{N}$ are chosen *independently*, hence $\langle h_i h_j \rangle_{\mathrm{RFC}} = R^2 \delta_{ij}$, where δ_{ij} is the Kronecker delta function, and $\langle ... \rangle_{\mathrm{RFC}}$ denotes the average over different random field configurations (RFC).

In the *nonequilibrium* zero-temperature RFIM, the system evolution is governed by the local relaxation rule: the spin S_i is stable while its sign is equal to the sign of *effective field*

$$h_i^{\mathrm{eff}} \equiv \sum_{\langle j \rangle} S_j + H + h_i, \tag{3}$$

where S_j are the nearest neighbors' spins of S_i; all spins that are unstable at the moment t of (discrete) time will flip in the next moment of time $t+1$ (parallel updating).

The flipping of each spin changes the effective field for all of its nearest neighbors. Those neighbors that become unstable will flip, which in turn may cause the flipping of their neighbors, and in this way an avalanche (of spin flipping) is created.

During each avalanche the value of H is kept constant here, so the system relaxes *adiabatically* towards some of its metastable states. The avalanche lasts until all spins become stable. After that, the only way to initiate the next avalanche is to change the value of the external field H.

Due to the foregoing *deterministic* rules, the system evolution is completely specified by the random field configuration $\{h_i\}_{i=1}^{N}$ of the quenched magnetic field, initial system state $\{S_i^0\}_{i=1}^{N}$, and the pattern of variation of external field H. The same applies to system response functions, like magnetization $M = (\sum_{i=1}^{N} S_i)/N$.

The system can be driven by the external field in various ways. Thus, starting from the initial condition $H = -\infty$ and all $S_i = -1$, one may simulate the rising part of the saturation hysteresis loop by increasing H exactly by the amount that flips the least stable spin, and repeat this until all $S_i = 1$. Alternatively, starting from $H = \infty$ and all $S_i = 1$, one may simulate the falling part by decreasing H until all $S_i = -1$.

In our simulations, the data were collected along the *rising* part of saturation hysteresis loop. The whole procedure, using different RFCs, is repeated many times until reliable statistics are collected.

III. SPANNING AVALANCHES

For any dimension $d > 1$, the nonequilibrium zero-temperature RFIM exhibits a critical behavior [2,7,8,11], separating two response regimes of *infinite* systems. If $R < R_c$, where $R_c = R_c(d)$ is the critical disorder, a jump in magnetization (i.e., the first-order phase transition) occurs, while for $R > R_c$ the magnetization varies smoothly with the external field H. At the critical disorder, $R = R_c$, the magnetization is still smooth, but with the infinite slope dM/dH at the critical field H_c.

The jumps in magnetization originate from the *spanning avalanches*: avalanches that span the *finite* system along at least one of its dimensions [9]. Spanning avalanches appear only if $R \leqslant R_c^{\mathrm{eff}}$, where $R_c^{\mathrm{eff}} = R_c^{\mathrm{eff}}(L,d)$ is the *effective* critical disorder for d-dimensional systems of linear size L; due to system finiteness, $R_c^{\mathrm{eff}}(L,d) > R_c$, and $R_c^{\mathrm{eff}}(L,d) \to R_c(d)$ in the thermodynamical limit $N \to \infty$.

The spanning avalanches are classified by the number of spatial dimensions they span [21]. So, in the 3D case, there are the one-dimensional (1D), 2D, and 3D-spanning avalanches, whereas in the 2D model there are only the 1D and 2D-spanning avalanches. The 3D-spanning avalanches in 3D model are further classified as subcritical and critical. The classification is based on the existence of two components forming the number distribution of 3D-spanning avalanches; see Fig. 4 in Ref. [21]. One component appears as a steplike function of disorder R decaying from one to zero in the vicinity of R_c and comprises almost compact 3D-spanning avalanches, called *subcritical*. The second component has the shape of a single peak near R_c and comprises less compact 3D-spanning avalanches, called *critical*; for more details see Sec. IV.

The analysis of spanning avalanches in 3D model revealed that all types of spanning avalanches influence the statistics of *finite* systems, but, for $R \neq R_c$, their contributions vanish when the system size $L \to \infty$; see Ref. [21]. The only exception comes from the subcritical 3D-spanning avalanches, which survive the thermodynamical limit for $R \leqslant R_c$, and for $R < R_c$ determine the behavior of the infinite system in its first-order phase transition. The case $R = R_c$ is more subtle because all types of spanning (and critical nonspanning) avalanches survive the $L \to \infty$ limit and contribute to the critical behavior.

During a single simulation of RFIM in $d \geqslant 3$ dimensions, more than one spanning avalanche may be triggered. This is not the case in the 2D model where, due to topology of of the lattice, periodic boundary conditions, and compactness of the spanning avalanches, at most one spanning avalanche per run may appear, so the hyperscaling relation [2,8,13]

$$d\nu - \beta = 1/\sigma, \tag{4}$$

violated for $d \geqslant 3$, holds in the 2D case; here ν describes the scaling $\xi \sim |r|^{1/\nu}$ of correlation length, β the scaling of magnetization jump $\Delta M \sim |r|^{\beta}$ below R_c, and σ the scaling of the largest avalanche size $S_{\max} \sim |r|^{\sigma}$ with reduced disorder $r \equiv (R - R_c)/R$.

IV. NUMERICAL ANALYSIS OF SPANNING AVALANCHES IN THE 2D MODEL

The spanning avalanches in the 2D model are extreme events that are realized at most once per run, and a huge number of runs is necessary to collect their reliable statistics. For this reason we have performed our simulations on 2D lattices that are, although smaller than in our previous papers [11,12], still large enough for the accomplishment of the current task [22,23].

In Fig. 1 we present $N_s(R,L)$, the average number per single run of spanning avalanches collected along the rising part of the saturation hysteresis loop, or simply the number of spanning avalanches, with the remark that the name of any other analogous quantity will be simplified similarly. Our data show that $N_s(R,L) \leqslant 1$ for any L and all R, and also that $N_s(R,L) = 1$ for small disorders and any lattice size L.

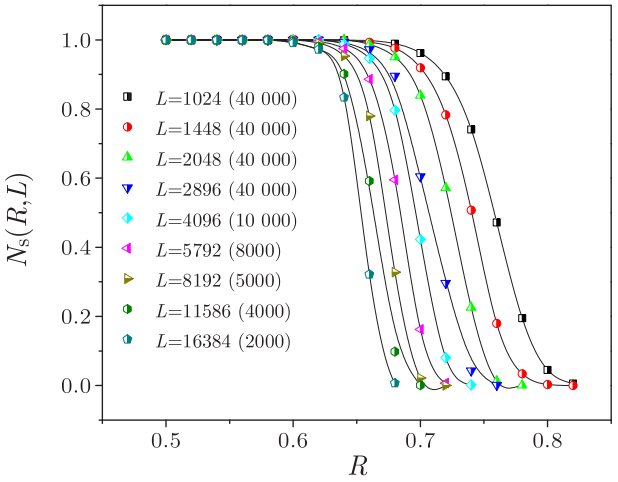

FIG. 1. (Color online) Number of spanning avalanches $N_s(R,L)$ as a function of disorder R for different system sizes L shown in the legend. The number $N_s(R,L)$ is estimated as $N_s(R,L) \approx N_s^{(\mathrm{reg})}(R,L)/N_{\mathrm{run}}$, where $N_s^{(\mathrm{reg})}(R,L)$ is the number of spanning avalanches registered in N_{run} simulations of the 2D model with different random field configurations for given R and L. The number of runs varied with L from 1000 to 40 000 and is shown in the legend for each L in parentheses.

A. Average number of 1D-spanning avalanches

The data in Fig. 1 correspond to *all* spanning avalanches. On the other hand, in analogy with the 3D model, the spanning avalanches of the 2D model can be classified as 1D-spanning and 2D-spanning avalanches. Thus, the 1D-spanning avalanches are those avalanches that span exactly one spatial dimension. In Fig. 2 we show the number of 1D-spanning avalanches $N_1(R,L)$. For each L, we found that $N_1(R,L)$, taken as function of R, can be well approximated by a Gaussian, and these Gaussians are shown by solid lines grouping individual data points with same L in Fig. 2. The

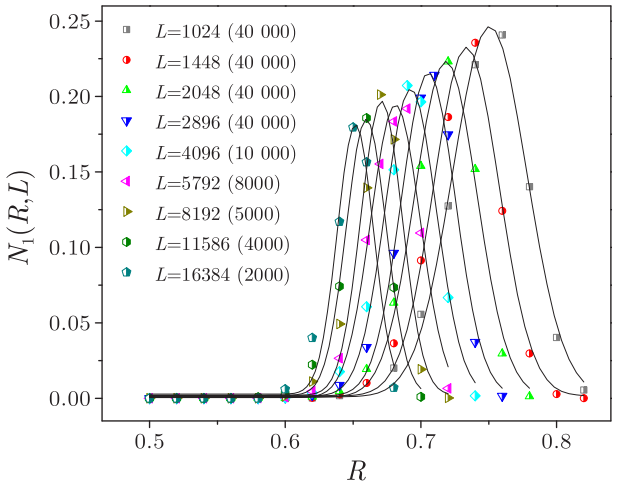

FIG. 2. (Color online) Number of 1D-spanning avalanches $N_1(R,L)$ against disorder R for lattice sizes L of 2D model and number of runs, given in parentheses. For each L, the connecting line shows the Gaussian that best fits the $N_1(R,L)$ data, taken as function of R.

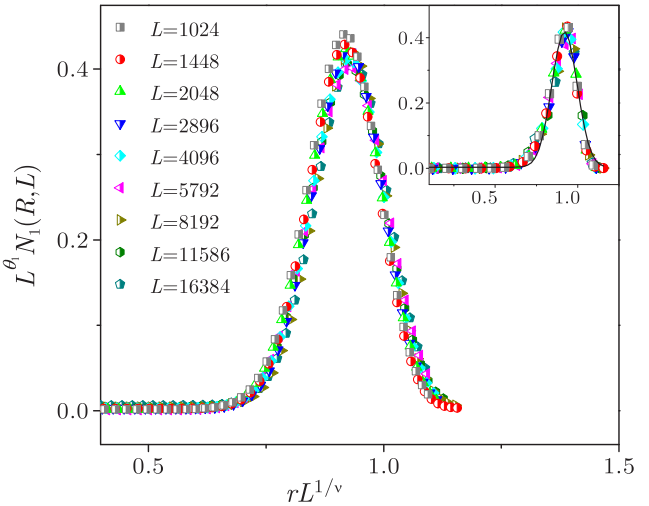

FIG. 3. (Color online) Main panel: Scaling collapse of the Gaussians from Fig. 2 that best fit the $N_1(R,L)$ data. The Gaussians are collapsed according to Eq. (5), and the parameters of the best collapse are $\theta_1 = 0.08 \pm 0.02$, $R_c = 0.54 \pm 0.02$, and $1/\nu = 0.192 \pm 0.006$. Inset: Number of 1D-spanning avalanches $N_1(R,L)$ collapsed using the same values of θ_1, R_c, and ν. The solid line shows the Gaussian that best fits the *collapsed* data and, therefore, estimates the form of the universal scaling function $\widetilde{N}_1(rL^{1/\nu})$.

height of the Gaussians decreases with L, suggesting that number of 1D-spanning avalanches $N_1(R,L)$ scales as

$$N_1(R,L) = L^{-\theta_1}\widetilde{N}_1(rL^{1/\nu}), \tag{5}$$

where θ_1 is the exponent of the number of 1D-spanning avalanches, $\widetilde{N}_1(x)$ is an universal scaling function of the single variable $x = rL^{1/\nu}$, and $r \equiv (R - R_c)/R$ is the reduced disorder commonly used in the RFIM context, and giving the same results in the $R \to R_c$ limit as the traditional reduced disorder $(R - R_c)/R_c$.

Expression (5) predicts that the scaled numbers of 1D-spanning avalanches, $N_1(R,L)L^{\theta_1}$, shown against the scaled reduced disorder $rL^{1/\nu}$, should fall on a single curve, provided that the exponents θ_1 and ν, as well as the critical disorder R_c, are properly chosen. The best scaling collapse of the foregoing type is presented in Fig. 3. In the main panel we show the collapsing of Gaussians that best fit the $N_1(R,L)$ data, shown in Fig. 2. The collapse is obtained for $\theta_1 = 0.08 \pm 0.02$, together with $R_c = 0.54 \pm 0.02$ and $1/\nu = 0.192 \pm 0.006$. In the inset, we show the raw $N_1(R,L)$ data, collapsed with the same parameter values θ_1, R_c, and ν. The collapsed data indicate that the universal scaling function $\widetilde{N}_1(x)$ has the maximum value $\simeq$0.42 at $x \simeq 0.92$, that its full width at half maximum (FWHM) is $\simeq$0.19, and that its form is roughly a Gaussian. In regard to the method of data collapsing, we would like to mention that all data collapses, presented in this paper, are performed with the aid of an algorithm [11,12] that minimizes the *collapse width* w, i.e., the width of the region that contains all scaled collapsing curves.

Far more important than data collapsing is that 1D-spanning avalanches are *irrelevant* in the thermodynamical limit of the 2D model. Indeed, for positive θ_1, expression (5) predicts that the number of 1D-spanning avalanches vanishes when the

system size $L \to \infty$, so the first-order phase transitions are only influenced by the 2D-spanning avalanches.

Finally, we would also like to point out that in the foregoing, and in all forthcoming data collapsing, we are using the reduced disorder $r = (R - R_c)/R$ as the scaling variable. As proposed in Ref. [21], better collapses are achieved using the scaling variable

$$u_2 \equiv \frac{R - R_c}{R_c} + A\left(\frac{R - R_c}{R_c}\right)^2, \tag{6}$$

but at the cost of an extra free parameter A, which we prefer to avoid.

B. Number of 2D-spanning avalanches

2D-spanning avalanches are the spanning avalanches that span the 2D system along both of its spatial dimensions. Due to the relatively small number of 1D-spanning avalanches, the number of 2D-spanning avalanches $N_2(R,L)$ is not much different from the corresponding number $N_s(R,L)$ of all spanning avalanches, shown in Fig. 1. For the sake of completeness, $N_2(R,L)$ is given in Fig. 4.

In the 3D model, the 3D spanning avalanches are classified as *critical* and *subcritical* [21]. The average number of subcritical 3D-spanning avalanches scales as $N_{3-}(R,L) = \widetilde{N}_{3-}(u_2 L^{1/\nu})$ and satisfies $N_{3-}(R,L) \leqslant 1$ because at most one subcritical avalanche can appear per single run. When $L \to \infty$ the number $N_{3-}(R,L)$ converges to $U(R_c - R)$, where $U(x)$ is the unit step function [$U(x) = 1$ for $x \geqslant 0$, and zero otherwise]. On the other hand, the number of *critical* 3D-spanning avalanches scales as $N_{3c}(R,L) = L^{\theta}\widetilde{N}_{3c}(u_2 L^{1/\nu})$, and *diverges* with L like the numbers of 1D-spanning avalanches, $N_1(R,L) = L^{\theta}\widetilde{N}_1(u_2 L^{1/\nu})$, and 2D-spanning avalanches, $N_2(R,L) = L^{\theta}\widetilde{N}_2(u_2 L^{1/\nu})$, the exponent θ being the same for all of them.

Different scaling with L of $N_{3-}(R,L)$ and $N_{3c}(R,L)$ *prevents* collapsing of the *overall* number of 3D-spanning avalanches $N_3(R,L) = N_{3-}(R,L) + N_{3c}(R,L)$ in the 3D case. Contrary to that, the number $N_2(R,L)$ of *all* 2D-spanning avalanches in the 2D model *collapse* on a single curve if the $N_2(R,L)$ data are scaled only along the horizontal axis and plotted against $rL^{1/\nu}$; see Fig. 5. This means that the $N_2(R,L)$ data scale as

$$N_2(R,L) = \widetilde{N}_2(rL^{1/\nu}), \tag{7}$$

and that $N_2(R,L)$ converges to the unit step function $U(R_c - R)$ in the $L \to \infty$ limit. Here $\widetilde{N}_2(rL^{1/\nu})$ is the corresponding single variable universal scaling function that we found can be approximated by the analytic expression

$$\widetilde{N}_2^{(a)}(x) = \widetilde{N}_{2c}^{(a)}(x) + \widetilde{N}_{2-}^{(a)}(x), \tag{8}$$

where

$$\widetilde{N}_{2c}^{(a)}(x) = H_G \exp[-(x - c)^2/2s^2] \tag{9}$$

is a Gaussian [of height $H_G = 0.3$, center $c = 0.89$, and $s = 0.08$, setting FWHM $= (2\sqrt{2\ln 2})s = 0.19$], while

$$\widetilde{N}_{2-}^{(a)}(x) = 0.5\,\mathrm{erfc}[7.6(x - 0.84)], \tag{10}$$

where $\mathrm{erfc}(x) \equiv (2/\sqrt{\pi})\int_x^{\infty} e^{-t^2} dt$ is the complementary error function; see Fig. 6.

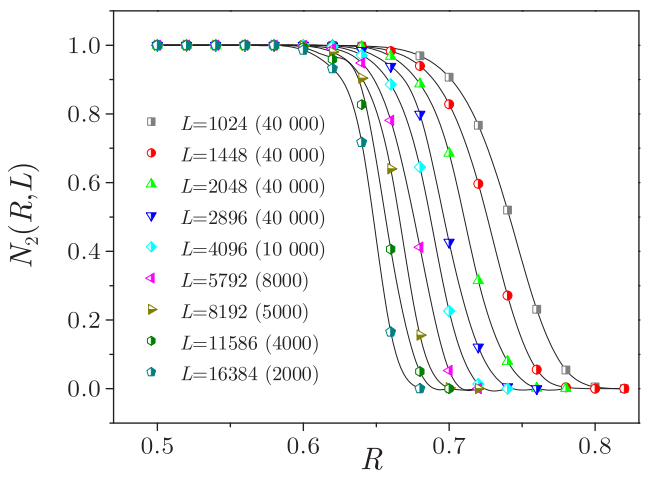

FIG. 4. (Color online) The number $N_2(R,L)$ of 2D-spanning avalanches in the 2D model against disorder R for various lattice sizes L and number of runs given in parentheses.

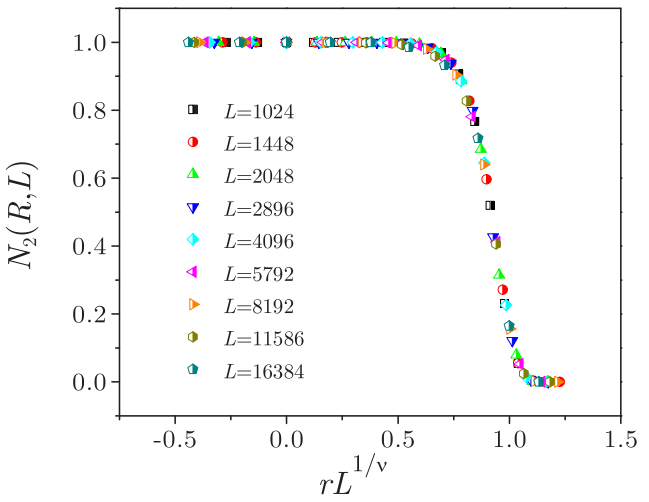

FIG. 5. (Color online) Scaling plot of the data from Fig. 4; the collapse is obtained for $R_c = 0.54$ and $1/\nu = 0.19$.

C. Fractal properties of spanning avalanches

Collapsing (7) of the $N_2(R,L)$ data indicates that if subcritical and critical 2D-spanning avalanches exist in the 2D case, then their numbers should scale with the zeroth power of L, namely,

$$N_{2-}(R,L) = \widetilde{N}_{2-}(rL^{1/\nu}) \tag{11}$$

and

$$N_{2c}(R,L) = \widetilde{N}_{2c}(rL^{1/\nu}), \tag{12}$$

where $\widetilde{N}_{2-}(x)$ and $\widetilde{N}_{2c}(x)$ are the corresponding universal scaling functions. For this reason the extraction of $N_{2-}(R,L)$ and $N_{2c}(R,L)$ from $N_2(R,L)$ data by the double finite-size scaling method, introduced in Ref. [21] for the 3D case, seems to be impossible here.

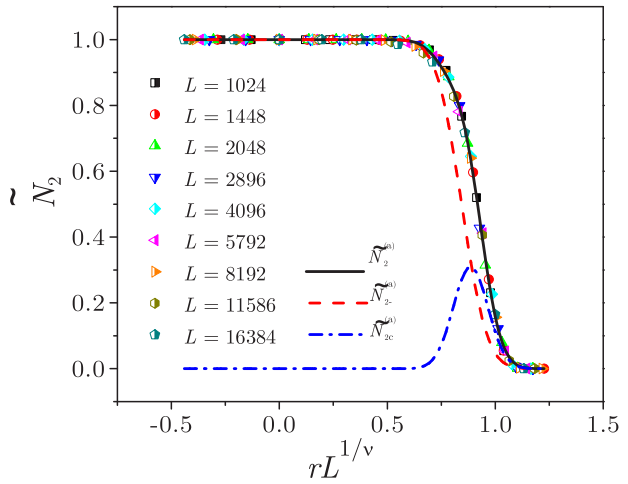

FIG. 6. (Color online) Universal scaling function $\widetilde{N}_2$ (symbols) and its analytic approximation $\widetilde{N}_2^{(a)}$ (solid line) plotted against $rL^{1/\nu}$; $R_c = 0.54$ and $1/\nu = 0.19$. The erfc component $\widetilde{N}_{2-}^{(a)}$ [see Eq. (10)] of the analytic approximation (8) is given by the dashed line, and the Gaussian component $\widetilde{N}_{2c}^{(a)}$ [see Eq. (9)] by the dash-dot line.

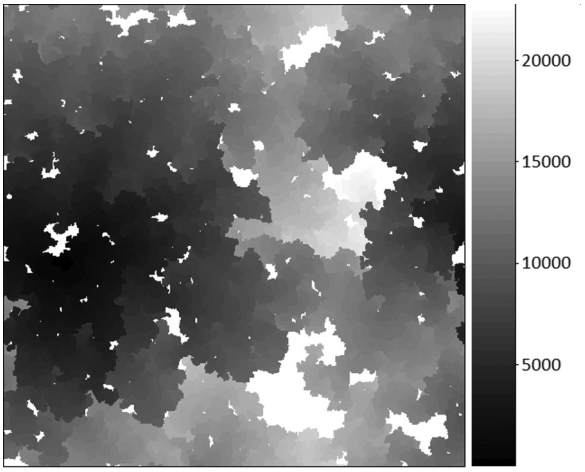

FIG. 8. Plot of a 2D-spanning avalanche in the 2D system. The avalanche is obtained for the same L and R as in Fig. 7, but with different configuration of quenched magnetic field h. The fractal dimension of the avalanche is $d_f = 1.9912$, and the avalanche is classified as *critical* by the $d_f^{(s)}$ method.

However, in Ref. [21] it was deduced that the subcritical and critical 3D-spanning avalanches have different *effective* fractal dimensions ($d_f = 2.98$ for subcritical, and $d_f = 2.78$ for other spanning and for critical nonspanning avalanches). So one may try to base their separation on the analysis of fractal dimension of individual spanning avalanches.

Large avalanches, and in particular spanning avalanches, triggered in simulations of RFIM are fractal objects. In Fig. 7 we give an example of a 1D-spanning avalanche, and in Figs. 8–9 two examples of 2D-spanning avalanches; all three avalanches are triggered in the same 2D system, and for the same values of R and L, but for different RFCs. The fractal dimensions of these three avalanches, as well as for all other individual avalanches, are estimated in our study by the box counting method; see, for instance, Ref. [24].

RFIM avalanches are statistical fractals characterized by the distribution of fractal dimension d_f of individual avalanches. The distribution of fractal dimension depends on the lattice dimension d and size L, disorder $R, \ldots$, as well as on the type of avalanches being analyzed. As an example, in Fig. 10 we show the distribution of fractal dimension of 2D-spanning avalanches triggered in a 2D system having linear size $L = 1024$ and disorder $R = 0.72$. One may notice that all 2D-spanning avalanches are quite compact ($d_f \approx 2$), and that the distribution of their fractal dimension is composed of two components; the left one is wider, bell-shaped, and centered around $d_f \approx 1.99$, and is continued to the right by a narrower component centered almost at $d_f = 2$.

The two-component structure of the fractal dimension distribution can be a sign that in the 2D model, like in

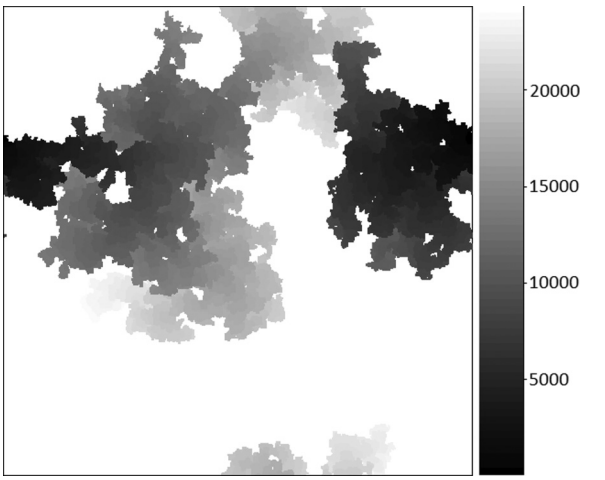

FIG. 7. Plot of a 1D-spanning avalanche in the 2D system: $L = 4096$, $R = 0.68$. The time scale of spin flipping is shown by the color legend; unaffected spins are white. Estimated fractal dimension of the avalanche is $d_f = 1.9828$.

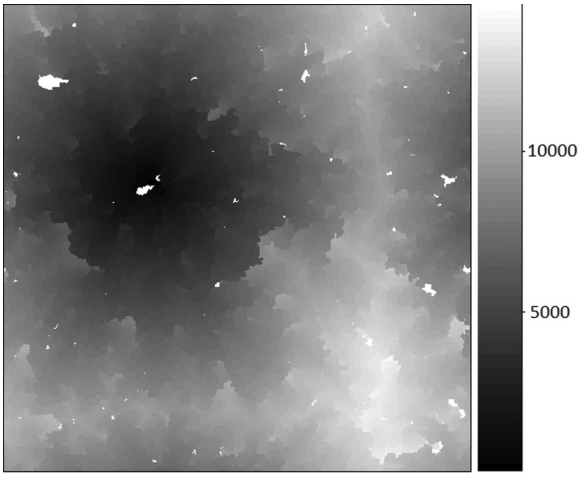

FIG. 9. Plot of a 2D-spanning avalanche in 2D system. L and R are the same as in Figs. 7–8, but the RFC is different. Estimated fractal dimension is $d_f = 1.9983$, and the avalanche is classified as *subcritical* by the $d_f^{(s)}$ method.

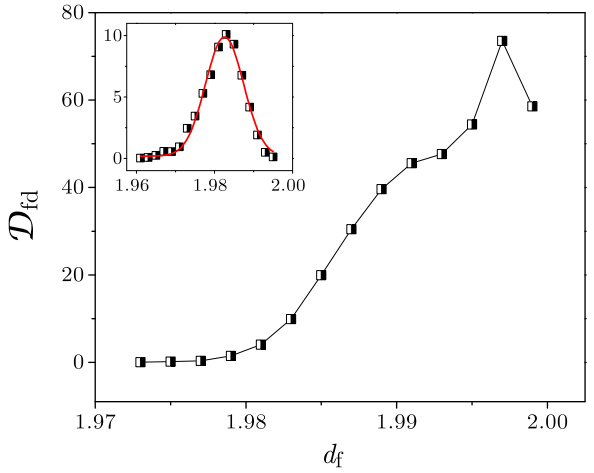

FIG. 10. (Color online) Distribution $\mathcal{D}_{\rm fd}$ of fractal dimension d_f of 2D-spanning avalanches in the 2D system with $L = 1024$ and $R = 0.72$. The area under the $\mathcal{D}_{\rm fd}$ curve is $N_2(R,L)$. In the present case, our choice for the value of $d_f^{(s)}$ is 1.9925, with the remark that other choices (e.g., between 1.991 and 1.994) are possible as well. Inset: The same, but for 1D-spanning avalanches, and the area equal to $N_1(R,L)$; solid line shows the best-fit Gaussian.

the 3D case, the spanning avalanches which span *all* spatial dimensions can be classified as *critical* and *subcritical*. The subcritical 2D-spanning avalanches are more compact and should contribute to $N_2(R,L)$ as the steplike distribution $N_{2-}(R,L)$ [see Eq. (11)] while the critical avalanches should correspond to $N_{2c}(R,L)$; [see Eq. (12)].

The crudest way to test the foregoing hypothesis is to select some value $d_f^{(s)}$ of fractal dimension that separates two components of the fractal dimension distribution (see Fig. 10) and to take as subcritical all 2D-spanning avalanches with fractal dimension $d_f \geqslant d_f^{(s)}$. The outcome of this $d_f^{(s)}$ method of classification is presented in Fig. 11. In the main panel we show that the average number of the avalanches which are classified as subcritical fall onto the analytic $\widetilde{N}_{2-}^{(a)}(rL^{1/\nu})$ curve, while the average number of the remaining (i.e., critical) 2D-spanning avalanches follow the $\widetilde{N}_{2c}^{(a)}(rL^{1/\nu})$ Gaussian [see inset (a)].

For a given system size L we have classified the 2D-spanning avalanches using the same value of $d_f^{(s)}$ for all disorders R. On the other hand, $d_f^{(s)}$ needs to change with L in order to stay adjusted with variation of fractal dimension distribution with the system size L. In inset (b) of Fig. 11 we show the currently used $d_f^{(s)}$ values versus $1/L$, indicating that $d_f^{(s)} \to 1.998$ when $L \to \infty$.

D. Nonspanning avalanches

The number of nonspanning avalanches $N_{\rm ns}(R,L)$ grows with both R and L; see Fig. 12 for the 2D case. In the absence of disorder the rising part of the saturation hysteresis loop should consist of a single avalanche in which all spins are flipped, so the number of avalanches must be 1 for all values of L. On the other hand, for large values of disorder, $R \gg R_c$, the system responds in a sequence of avalanches of size 1,

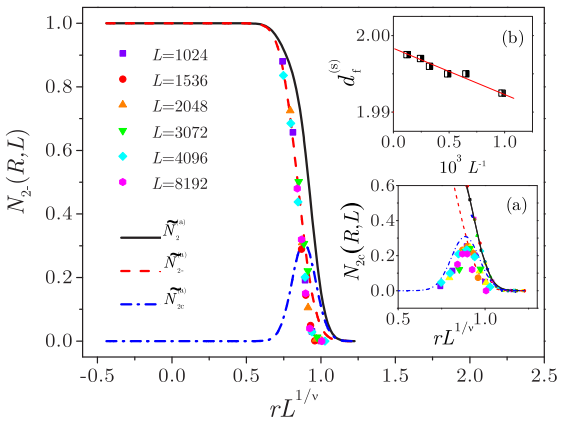

FIG. 11. (Color online) Main panel: Number of *subcritical* 2D-spanning avalanches $N_{2-}(R,L)$ versus $rL^{1/\nu}$; $R_c = 0.54$ and $1/\nu = 0.19$. The collapsed data points (symbols) should fall onto the universal scaling function $\widetilde{N}_{2-}(rL^{1/\nu})$ of *subcritical* 2D-spanning avalanches. Like in Fig. 6, the solid line shows the analytical approximation $\widetilde{N}_2^{(a)}$ [see Eq. (8)] of the universal scaling function $\widetilde{N}_2(rL^{1/\nu})$ of *all* 2D-spanning avalanches (7), the dashed line the erfc component $\widetilde{N}_{2-}^{(a)}$ of $\widetilde{N}_2^{(a)}$ [see Eq. (10)], and the dash-dot line the Gaussian component $\widetilde{N}_{2c}^{(a)}$ of $\widetilde{N}_2^{(a)}$ [see Eq. (9)]. Insets: (a) the same as in the main panel, but for the *critical* 2D-spanning avalanches; (b) separation values $d_f^{(s)}$ of fractal dimension versus reciprocal system size $1/L$.

and therefore the number of nonspanning avalanches should be equal to the number of spins N. For all other values of disorder, the role of very small avalanches is to prepare the terrain for the emergence of larger and, in particular, spanning avalanches. Although smaller than N, the number of such avalanches scales with N, so one may guess that the number of *all* nonspanning avalanches should scale with $N = L^d$ as

$$N_{\rm ns}(R,L) = L^d \widetilde{N}_{\rm ns}(R), \tag{13}$$

which is in reasonable agreement with our 2D data; see Fig. 13.

Note, however, that a detailed analysis [21] has revealed that the simple scaling (13) is not entirely appropriate in the 3D model. The cause can be traced back to the contribution of

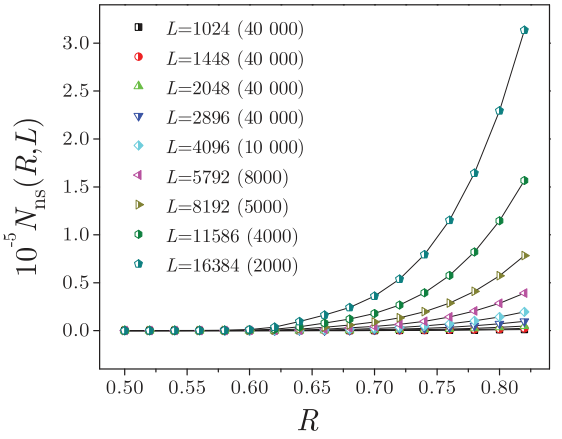

FIG. 12. (Color online) Number of nonspanning avalanches $N_{\rm ns}(R,L)$ in the 2D model against disorder R for various system sizes L and number of runs quoted in parentheses.

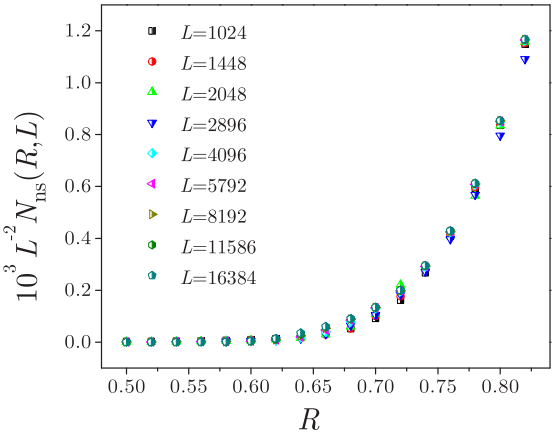

FIG. 13. (Color online) Scaled number of nonspanning avalanches $N_{ns}(R,L)$ against disorder R for various sizes L of the 2D system.

large nonspanning avalanches, called *critical*, whose number diverges as $L^{\theta_{nsc}}\tilde{N}_{nsc}(uL^{1/\nu})$ with exponent $\theta_{nsc} < 3$. The number of analogous nonspanning avalanches in the 2D model seems to vanish when $L \to \infty$, and that might be the reason why the simple scaling (13) works better in the 2D case.

V. SCALING OF THE SPANNING AVALANCHE SIZE DISTRIBUTIONS

Spanning avalanches contribute to various avalanche distributions which will be elaborated here in the case of avalanche size distributions in the 2D model.

In panel (a) of Fig. 14, we show the size distribution $D'(S,R,L)$ of *all* avalanches versus relative avalanche size S/L^2, i.e., size S divided by the maximum size L^2. The distribution pertains to $L = 2896$ and disorder $R = 0.70$, which is below the effective critical disorder $R_c^{\rm eff}$ for that L. Here $D'(S,R,L)$ is scaled so that $\sum_S D'(S,R,L) = N_{av}$, where N_{av} is the average number per single run of *all* avalanches, registered along the rising part of the saturation hysteresis loop. Therefore, $D'(S,R,L) = N_{av}D(S,R,L)$, where $D(S,R,L)$ is the probability density function (PDF) of size distribution, alternatively, *normalized* size distribution, satisfying $\sum_S D(S,R,L) = 1$.

Almost throughout the whole range of avalanche size, $D'(S,R,L)$ coincides with the sizes distribution $D'_{ns}(S,R,L) = N_{ns}D_{ns}(S,R,L)$ of *nonspanning* avalanches [see panel (a) in Fig. 14]; N_{ns} is the number and $D_{ns}(S,R,L)$, normalized size distribution of nonspanning avalanches. Note that the right-hand cutoff of $D'_{ns}(S,R,L)$ is rather sharp. So, the number of *critical* nonspanning avalanches must be small, and this enables the simple scaling (13).

The contribution of spanning avalanches is manifested as a peak at the large-size end of the distribution $D'(S,R,L)$. In panel (b) of Fig. 14, we present in the relevant range of avalanche size S the size distribution $D'_s(S,R,L) = N_s D_s(S,R,L)$ of *spanning* avalanches, together with its two components: size distribution $D'_1(S,R,L) = N_1 D_1(S,R,L)$ of 1D-spanning avalanches, and size distribution $D'_2(S,R,L) = N_2 D_2(S,R,L)$ of 2D-spanning avalanches; N_s, N_1, and N_2 are the numbers, while D_s, D_1, and D_2 are the normalized size distributions of spanning, 1D-spanning, and 2D-spanning avalanches, respectively. Finally, one can follow the size distributions $D'_{2c}(S,R,L) = N_{2c}D_{2c}(S,R,L)$ and $D'_{2-}(S,R,L) = N_{2-}D_{2-}(S,R,L)$ of critical and subcritical 2D-spanning avalanches, together with their normalized versions $D_{2c}(S,R,L)$ and $D_{2-}(S,R,L)$.

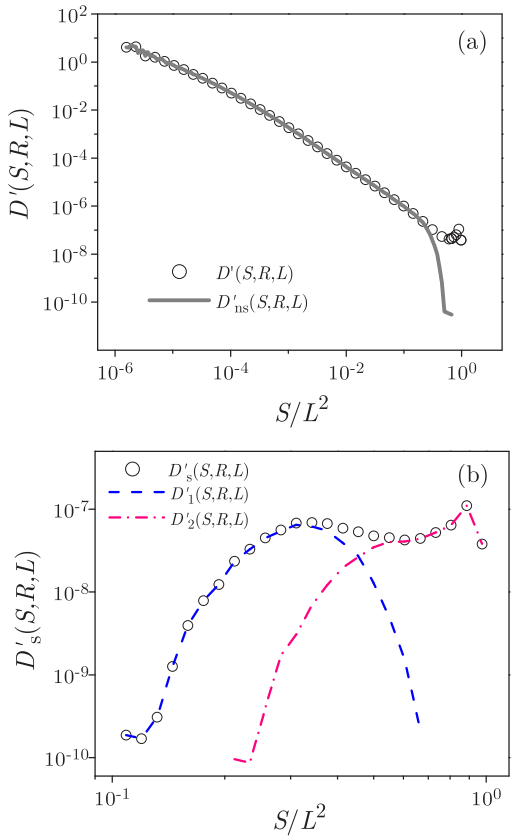

FIG. 14. (Color online) Avalanche size distributions versus relative avalanche size S/L^2, i.e., avalanche size S divided by the maximum avalanche size L^2 in the 2D model; $L = 2896$ and $R = 0.70$. (a) Distribution $D'(S,R,L)$ of *all* avalanches (circles), and distribution $D'_{ns}(S,R,L)$ of nonspanning avalanches (solid line). (b) Distribution $D'_s(S,R,L)$ of spanning avalanches (circles) and its two components: distribution $D'_1(S,R,L)$ of 1D-spanning avalanches (dashed line), and distribution $D'_2(S,R,L)$ of 2D-spanning avalanches (dash-dot line).

The foregoing size distributions satisfy some relations which become particularly simple with the adopted choice of their normalization. In this case the distribution relations read

$$D'(S,R,L) = D'_{ns}(S,R,L) + D'_s(S,R,L), \quad (14)$$

$$D'_s(S,R,L) = D'_1(S,R,L) + D'_2(S,R,L), \quad (15)$$

$$D'_2(S,R,L) = D'_{2c}(S,R,L) + D'_{2-}(S,R,L)\,. \quad (16)$$

which is suitable for visual inspection. On the other hand, it is more convenient to use normalized distributions for the forthcoming scaling analysis.

Normalized size distribution $D_1(S,R,L)$ of 1D-spanning avalanches scales with avalanche size S as

$$D_1(S,R,L) = L^{-\tau_1 d_f^{(1)}} \widetilde{D}_1\left(SL^{-d_f^{(1)}}, rL^{1/\nu}\right), \qquad (17)$$

where τ_1 is the size exponent, $d_f^{(1)}$ is the *effective* fractal dimension, and $\widetilde{D}_1$ is the universal scaling function, all for 1D-spanning avalanches. Similarly, for the normalized size distribution $D_{2c}(S,R,L)$ of critical 2D-spanning avalanches, one can propose the scaling

$$D_{2c}(S,R,L) = L^{-\tau_{2c} d_f^{(2c)}} \widetilde{D}_{2c}\left(SL^{-d_f^{(2c)}}, rL^{1/\nu}\right) \qquad (18)$$

described by the size exponent τ_{2c} and effective fractal dimension of critical 2D-spanning avalanches, and likewise the scaling

$$D_{2-}(S,R,L) = L^{-\tau_{2-} d_f^{(2-)}} \widetilde{D}_{2-}\left(SL^{-d_f^{(2-)}}, rL^{1/\nu}\right) \qquad (19)$$

for subcritical 2D-spanning avalanches, characterized by analogous exponents τ_{2-} and $d_f^{(2-)}$. If the normalized distributions D_1, D_{2c}, and D_{2-} rapidly tend to zero on both of their ends, then one can show (see Ref. [21]) that

$$\tau_1 = \tau_{2c} = \tau_{2-} = 1, \qquad (20)$$

so the scaling laws (17)–(19) of the size distributions in question are determined only by the corresponding values of effective fractal dimensions.

In Fig. 15 we show the collapse (17) of the *normalized* avalanche size distributions $D_1(S,R,L)$, obtained for the best values of free collapse parameters $d_f^{(1)} = 1.96$ and $\tau_1 = 0.99$, and for $rL^{1/\nu} = \text{const}$ with fixed $R_c = 0.54$ and $1/\nu = 0.19$. The collapsed data indicate that the universal scaling function $\widetilde{D}_1(x,y)$ is a bell-shaped function of the first variable $x = SL^{-d_f^{(1)}}$ for the fixed value of the second variable $y = rL^{1/\nu}$.

Having at our disposal the $d_f^{(s)}$ method for classification of 2D-spanning avalanches into subcritical and critical, we have also checked the scaling hypotheses (18) and (19), and the collapses are shown in Figs. 16–17. Despite these collapses, due to the rather coarse method of avalanche classification, are not as good as in Fig. 15, we consider that they agree with Eqs. (18)–(20) and provide reasonable estimation of the effective fractal dimensions.

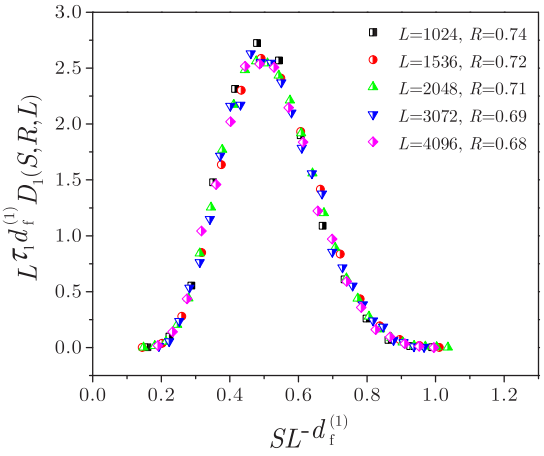

FIG. 15. (Color online) Scaling plot of the *normalized* size distribution $D_1(S,R,L)$ of 1D-spanning avalanches. The best data collapse is obtained under $rL^{1/\nu} = \text{const}$ conditions ($1/\nu = 0.19$, $R_c = 0.54$), and for the values of free collapse parameters $\tau_1 = 0.99 \pm 0.02$ and $d_f^{(1)} = 1.96 \pm 0.02$.

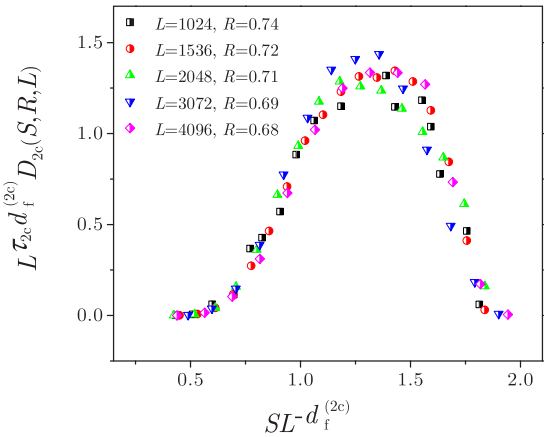

FIG. 16. (Color online) Scaling plot of *normalized* size distribution of *critical* 2D-spanning avalanches. The collapse is obtained under same conditions as in Fig. 15, and for the values of free collapse parameters $\tau_{2c} = 1.00 \pm 0.03$ and $d_f^{(2c)} = 1.92 \pm 0.04$.

VI. MAGNETIZATION JUMPS

For very large systems, magnetization jumps ΔM originate from the spanning avalanches. In the 2D model, the jump of magnetization, *averaged* over different random field configurations, reads

$$\langle \Delta M \rangle = \frac{2}{L^2} N_s \langle S \rangle_s, \qquad (21)$$

where N_s is the average number of spanning avalanches per single run, and $\langle S \rangle_s$ is the average size of spanning avalanches [25]. The product $N_s \langle S \rangle_s$ is the sum

$$N_s \langle S \rangle_s = N_1 \langle S \rangle_1 + N_{2-} \langle S \rangle_{2-} + N_{2c} \langle S \rangle_{2c} \qquad (22)$$

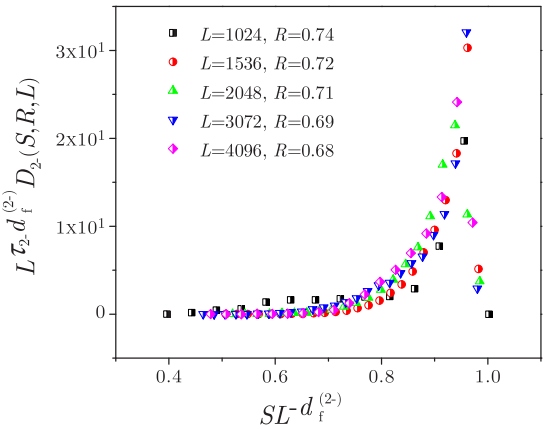

FIG. 17. (Color online) Scaling plot of *normalized* size distribution of *subcritical* 2D-spanning avalanches. The collapse is obtained under the same conditions as in Figs. 15 and 16, and for the values $\tau_{2-} = 1.04 \pm 0.06$ and $d_f^{(2-)} = 2.00 \pm 0.05$ of the free collapse parameters.

of contribution $N_1\langle S\rangle_1$ of 1D-spanning avalanches, and contributions $N_{2-}\langle S\rangle_{2-}$ and $N_{2c}\langle S\rangle_{2c}$ of subcritical and critical 2D-spanning avalanches. Here, because the normalized size distributions $D_\alpha(S,R,L)$ rapidly tend to zero on both of their ends, each $\langle S\rangle_\alpha = \sum_S S D_\alpha(S,R,L)$ scales with the effective fractal dimension $d_f^{(\alpha)}$ as

$$\langle S\rangle_\alpha = L^{d_f^{(\alpha)}}\Psi_\alpha(rL^{1/\nu}), \tag{23}$$

where $\Psi_\alpha(rL^{1/\nu}) \equiv \int_0^\infty x\widetilde{D}_\alpha(x,rL^{1/\nu})$. Hence,

$$\begin{aligned} N_s\langle S\rangle_s = {} & L^{d_f^{(1)}-\theta}\widetilde{N}_1(rL^{1/\nu})\Psi_1(rL^{1/\nu}) \\ & + L^{d_f^{(2-)}}\widetilde{N}_{2-}(rL^{1/\nu})\Psi_{2-}(rL^{1/\nu}) \\ & + L^{d_f^{(2c)}}\widetilde{N}_{2c}(rL^{1/\nu})\Psi_{2c}(rL^{1/\nu}), \end{aligned} \tag{24}$$

and for large L it simplifies to

$$N_s\langle S\rangle_s \approx L^2\widetilde{N}_{2-}(rL^{1/\nu})\Psi_{2-}(rL^{1/\nu}), \tag{25}$$

because $d_f^{(2-)} = 2$, and because $\theta > 0$ and both $d_f^{(1)}$ and $d_f^{(2c)}$ are less than two.

Therefore, we propose the simple scaling

$$\langle\Delta M\rangle = \widetilde{\Delta M}(rL^{1/\nu}) \tag{26}$$

of magnetization jump of large 2D systems, where

$$\widetilde{\Delta M}(rL^{1/\nu}) \equiv 2\widetilde{N}_{2-}(rL^{1/\nu})\Psi_{2-}(rL^{1/\nu}) \tag{27}$$

is the corresponding universal scaling function of the single variable $rL^{1/\nu}$.

The scaling prediction (26) implies that the magnetization jump data should collapse onto a single curve after being scaled only along the horizontal axis. This is in agreement with our simulation data, and evidenced in the main panel of Fig. 18 by the magnetization jumps, collapsed according to prediction (26); noncollapsed data are shown in the inset.

VII. ANALYSIS OF SPANNING FIELD

In order to obtain additional insight into the role of spanning avalanches, we introduce an analysis of their spanning fields.

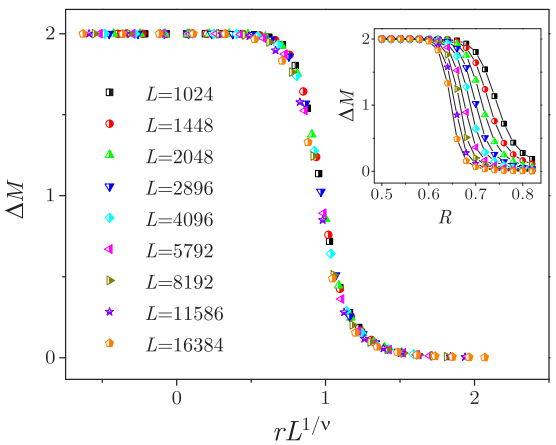

FIG. 18. (Color online) Main panel: Magnetization jumps ΔM against $rL^{1/\nu}$; $R_c = 0.54$ and $1/\nu = 0.19$. The collapsed curves are obtained in 2D model for lattice sizes L given in legend. Inset: Main panel data against disorder R.

For each spanning avalanche one can monitor its *spanning field* $H_{\rm sp}$, the value of the external magnetic field which triggers this avalanche. The spanning field is a random variable determined by the overall simulation conditions, and in particular by the choice of the random field configuration.

In Fig. 19 we present three examples of the spanning field raw distributions, collected for different values of disorder R in the case of the 2D system. For each R the distribution is narrow and concentrated around the *effective* critical field $H_c^{\rm eff}(R)$, the value of the external magnetic field H for which the *averaged* magnetization curve for disorder R exhibits the steepest variation with H. When $R \to R_c$, $H_c^{\rm eff}(R)$ tends to the *critical* field H_c of the 2D model, and for the small reduced disorder r

$$H_c^{\rm eff}(r) \approx H_c - br, \tag{28}$$

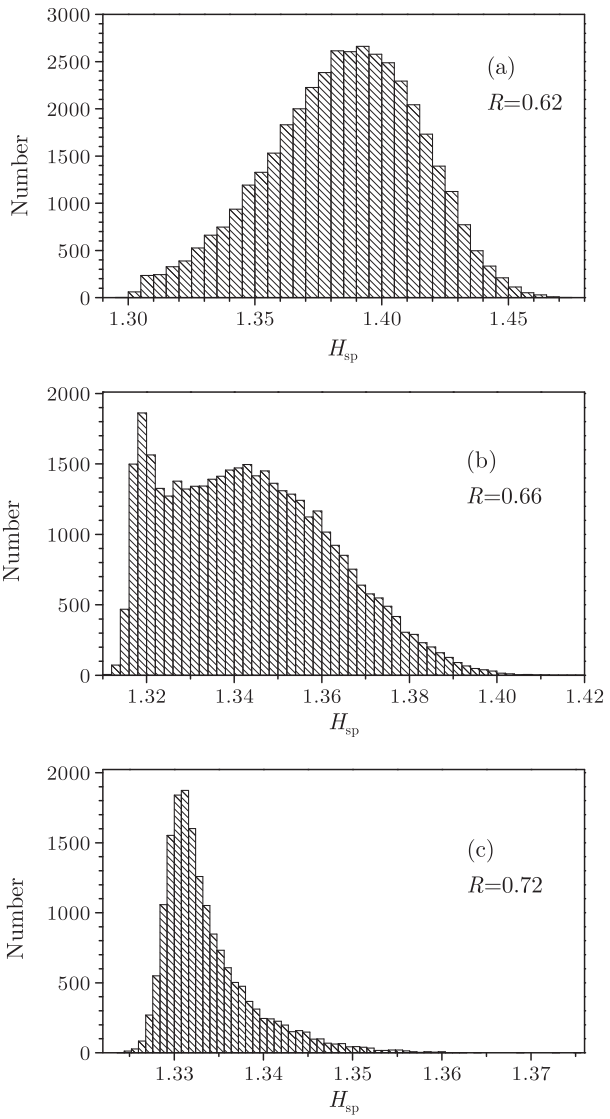

FIG. 19. Raw distributions of spanning field $H_{\rm sp}$ in the case of 2D system with $L = 2896$. The distributions are collected in 40 000 simulations for each of three values of disorder R indicated in the legends.

where the "rotation" parameter b controls the shift of $H_c^{(\mathrm{eff})}$ relative to H_c; see Refs. [2,8,9]. In the 2D model, we found [11,12] that $R_c = 0.54$, $H_c = 1.275$, and $b = 0.24$.

According to the type of triggered spanning avalanche, we classify the realizations of spanning field H_{sp} as 1D and 2D, and 2D spanning field realizations into subcritical and critical. The corresponding distribution $N'_\alpha(H_{\mathrm{sp}};R,L)$ of α type of spanning field H_{sp} depends parametrically on disorder R and lattice size L and is normalized so that

$$\int_{-\infty}^{+\infty} N'_\alpha(H_{\mathrm{sp}};R,L)dH_{\mathrm{sp}} = N_\alpha(R,L), \tag{29}$$

where $N_\alpha(R,L)$ is the average number per single run of spanning avalanches of type α. Such distributions satisfy

$$N'_s(H;R,L) = N'_1(H;R,L) + N'_2(H;R,L), \tag{30}$$

where $N'_s(H;R,L)$ counts the number of *all* spanning fields regardless of their type (cf. Fig. 19) and

$$N'_2(H;R,L) = N'_{2-}(H;R,L) + N'_{2c}(H;R,L)\,. \tag{31}$$

Taking into account scaling relation (5), we propose that the distribution $N'_1(H;R,L)$ scales as

$$N'_1(H;R,L) = L^{\zeta_1-\theta_1}\widetilde{N}'_1(h'L^{\zeta_1},rL^{1/\nu})\,. \tag{32}$$

Here ζ_1 is the exponent of the 1D-spanning field, $\widetilde{N}'_1(h'L^{\zeta_1},rL^{1/\nu})$ is the corresponding universal scaling function of two variables, $x = h'L^{\zeta_1}$, and $y = rL^{1/\nu}$, while the *reduced* magnetic field [2,8,9,11,12]

$$h' = H - H_c^{(\mathrm{eff})}(r) \tag{33}$$

is calculated for $H = H_{\mathrm{sp}}$.

In Fig. 20 we show the distributions $N'_1(H;R,L)$, collapsed according to scaling prediction (32). The displayed distributions correspond to four combinations of disorder R and lattice size L satisfying the scaling condition $rL^{1/\nu} = \mathrm{const}$. With fixed values $\theta_1 = 0.08$ and $1/\nu = 0.19$, the best collapse is obtained for the value $\zeta_1 = 0.77 \pm 0.02$ of exponent ζ_1, pertaining to distribution $N'_1(H;R,L)$ of the 1D-spanning field. In the same figure we also show a Gaussian approximation of the corresponding universal scaling function $\widetilde{N}'_1(h'L^{\zeta_1},rL^{1/\nu})$, which is for the $rL^{1/\nu} = \mathrm{const}$ function of the single variable $h'L^{\zeta_1}$.

In an analogous way, we propose that the distributions of subcritical and critical 2D-spanning field scale as

$$N'_{2-}(H;R,L) = L^{-\zeta_2}\widetilde{N}'_{2-}(h'/L^{\zeta_2},rL^{1/\nu}), \tag{34}$$

$$N'_{2c}(H;R,L) = L^{-\zeta_2}\widetilde{N}'_{2c}(h'/L^{\zeta_2},rL^{1/\nu})\,, \tag{35}$$

where $\widetilde{N}'_{2-}(h'/L^{\zeta_2},rL^{1/\nu})$ and $\widetilde{N}'_{2c}(h'/L^{\zeta_2},rL^{1/\nu})$ are the corresponding universal scaling functions for the subcritical and critical 2D-spanning fields, respectively. Note that the exponent ζ_2 of the 2D-spanning fields is the *same* in both scaling relations, so the distribution $N'_2(H;R,L)$ of *all* realizations of the 2D-spanning field manifests scaling

$$N'_2(H;R,L) = L^{-\zeta_2}\widetilde{N}'_2(h'/L^{\zeta_2},rL^{1/\nu}), \tag{36}$$

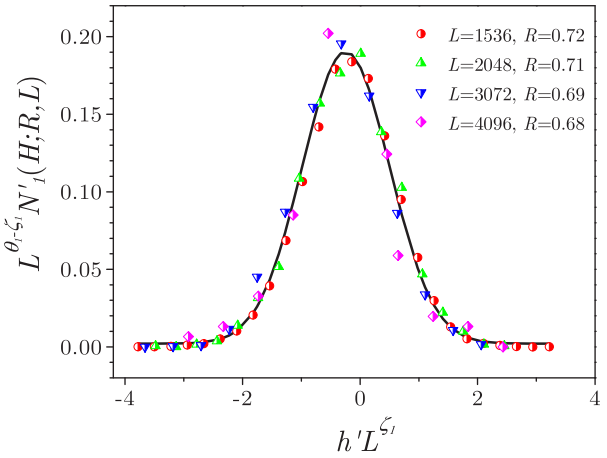

FIG. 20. (Color online) Scaling plot of distributions $N'_1(H;R,L)$ of a 1D-spanning field (symbols) versus combination $h'L^{\zeta_1}$ of variables L and h', where $h' = H_{\mathrm{sp}} - H_c - br$ is the reduced value of a 1D-spanning field H_{sp} [see Eq. (33)]. The R,L pairs of displayed distributions satisfy $rL^{1/\nu} \approx \mathrm{const}$ and are shown in the legend. The best collapse with fixed $\theta_1 = 0.08$ is obtained for $\zeta_1 = 0.77 \pm 0.02$. The full line shows the Gaussian $H_G \exp[-(x-c)^2/2s^2]$, which approximates the universal scaling function of 1D-spanning field $\widetilde{N}'_1(h'L^{\zeta_1},rL^{1/\nu})$ for $rL^{1/\nu} = \mathrm{const}$; the Gaussian parameters are height $H_G = 0.19$, center $c = -0.24$, and FWHM $= (2\sqrt{2\ln 2})s = 1.74$.

described by the universal scaling function

$$\widetilde{N}'_2(h'/L^{\zeta_2},rL^{1/\nu}) = \widetilde{N}'_{2-}(h'/L^{\zeta_2},rL^{1/\nu}) + \widetilde{N}'_{2c}(h'/L^{\zeta_2},rL^{1/\nu})\,. \tag{37}$$

In Fig. 21 we show the distributions of all realizations of the 2D-spanning field $N'_2(H;R,L)$, scaled according to prediction (36). The displayed $N'_2(H;R,L)$ data are collected in the same set of simulations as the $N'_1(H;R,L)$ distributions, shown in Fig. 20. Their best collapse, with exponent ζ_2 as the single free collapse parameter, is obtained for the value $\zeta_2 = -0.30 \pm 0.02$.

The best analytical approximation of the universal scaling function $\widetilde{N}'_2(h'/L^{\zeta_2},rL^{1/\nu})$ with $rL^{1/\nu} = \mathrm{const}$ is also shown in Fig. 21. It has the form of exponentially modified Gaussian (EMG) function

$$\mathrm{EMG}(x) = \frac{A}{2\mu}\exp\left(\frac{s^2}{2\mu^2}+\frac{c-x}{\mu}\right)\mathrm{erfc}\left(\frac{s^2/\mu+c-x}{\sqrt{2}s}\right), \tag{38}$$

which is the convolution

$$\mathrm{EMG}(x) = (G_A * E)(x), \tag{39}$$

of the Gaussian function

$$G_A(x) = \frac{A}{s\sqrt{2\pi}}\exp\left[-\frac{(x-c)^2}{2s^2}\right] \tag{40}$$

[having the FWHM $= (2\sqrt{2\ln 2})s$ around the center c, and enclosing the area A under its graph] with the exponential

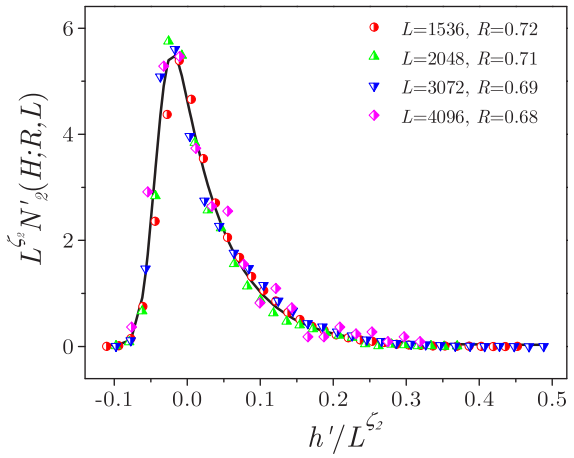

FIG. 21. (Color online) Scaling plot of distributions $N'_2(H;R,L)$ of *all* realizations of the 2D-spanning field (symbols) versus combination h'/L^{ζ_2} of variables L and h', where $h' = H_{sp} - H_c - br$ is the reduced value of the 2D-spanning field H_{sp} [see Eq. (33)]. The R,L pairs of displayed distributions satisfy $rL^{1/\nu} \approx$ const and are shown in the legend. The best collapse is obtained for $\zeta_2 = -0.30 \pm 0.02$. The full line shows the exponentially modified Gaussian function (EMG) [see Eq. (38)], which approximates the universal scaling function of the 2D-spanning field $\widetilde{N}'_2(h'/L^{\zeta_2}, rL^{1/\nu})$ for $rL^{1/\nu} =$ const. The EMG parameters are $A = 0.56$, $c = -0.04$, $s = 0.016$, and $\mu = 0.065$.

distribution

$$E(x) = \begin{cases} \mu^{-1} \exp(-x/\mu), & x \geqslant 0 \\ 0, & x < 0 \end{cases} \qquad (41)$$

specified by the characteristic value μ of its argument x.

Distribution $N'_{2-}(H;R,L)$ of the *subcritical* 2D-spanning field, extracted with the aid of the $d_f^{(s)}$ method of classification of 2D-spanning avalanches, is very similar to the distribution $N'_2(H;R,L)$ of all realizations of the 2D-spanning field. The collapse of $N'_{2-}(H;R,L)$ data, carried out with the same value of ζ_2, is shown in panel (a) of Fig. 22, together with the EMG approximation of the universal scaling function $\widetilde{N}'_{2-}(h'/L^{\zeta_2}, rL^{1/\nu})$ of the subcritical 2D-spanning field. On the other hand, the universal scaling function $\widetilde{N}'_{2c}(h'/L^{\zeta_2}, rL^{1/\nu})$ of the *critical* 2D-spanning field has a Gaussian shape, which is suggested by the collapse of distributions $N'_{2c}(H;R,L)$ of the *critical* 2D-spanning field, given in panel (b) of Fig. 22.

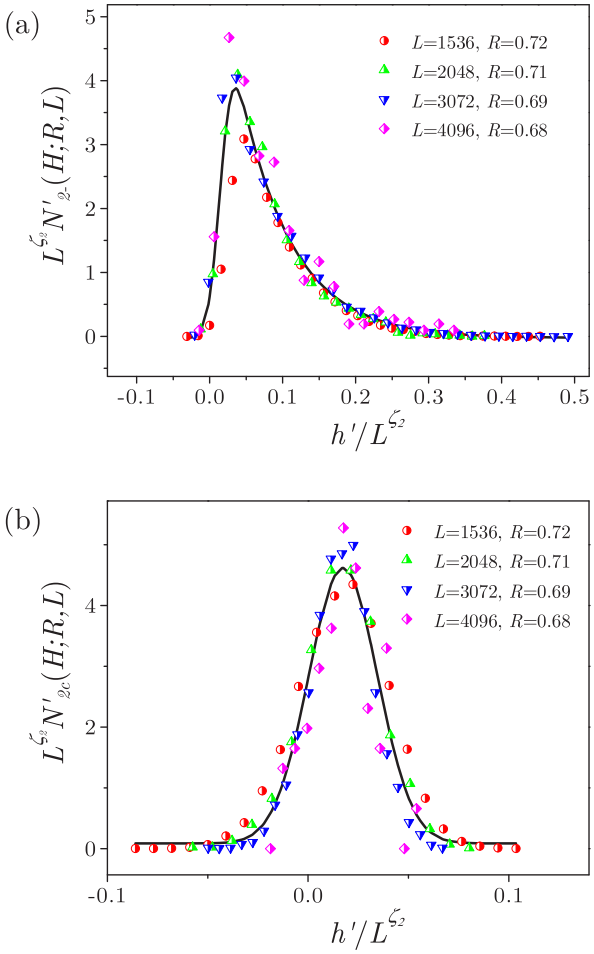

FIG. 22. (Color online) (a) The same as in Fig. 21, but for the distribution $N'_{2-}(H;R,L)$ of *subcritical* 2D-spanning field. (b) The scaling collapse of the distribution $N'_{2c}(H;R,L)$ of *critical* 2D-spanning field obtained for the same value of exponent ζ_2 as in panel (a) and in Fig. 21. The full line shows the Gaussian that best fits the collapsed $N'_{2c}(H;R,L)$ data and approximates the corresponding universal scaling function $\widetilde{N}'_{2c}(h'/L^{\zeta_2}, rL^{1/\nu})$ for $rL^{1/\nu} =$ const.

VIII. COLLAPSING OF MAGNETIZATION CURVES BELOW CRITICAL DISORDER

For the values of disorder below *effective* critical disorder $R_c^{\text{eff}}(L)$, each magnetization curve that is realized by a *single* random field configuration displays jump(s) generated by spanning avalanche(s). In the 2D model, on each such curve there is a single jump located at $H = H_{sp}$, i.e., at the value of the spanning field H_{sp} that is triggering the single spanning avalanche for the employed random field configuration.

In the main panel of Fig. 23 we show several examples of single random field configuration (RFC) magnetization curves, obtained on the same 2D lattice, but for different values of disorder R. Except at jump points, they appear as smooth curves on the current scale. The curves are virtually of rectangular shape, because almost all spins are flipped in the pertaining single spanning avalanche.

Due to the stochastic nature of the spanning field, single RFC magnetization jumps appear at different values of the external field H, covering a narrow range around the *effective* critical field $H_c^{(\text{eff})}$. Therefore, the middle part of the *averaged* magnetization curve, obtained by averaging over different RFCs, has visible steps if the number of employed RFCs is small; see the inset in Fig. 1 of Ref. [11]. On the other hand, if the averaged magnetization curve is obtained from a *large* number of RFCs, the steps disappear, and the distribution of vertical jumps, pertaining to single RFC curves, causes a finite ascent in the middle part of the averaged curve; see the inset in Fig. 23.

The averaged magnetization comprises two contributions,

$$M(H;R,L) = M_s(H;R,L) + M_{ns}(H;R,L), \qquad (42)$$

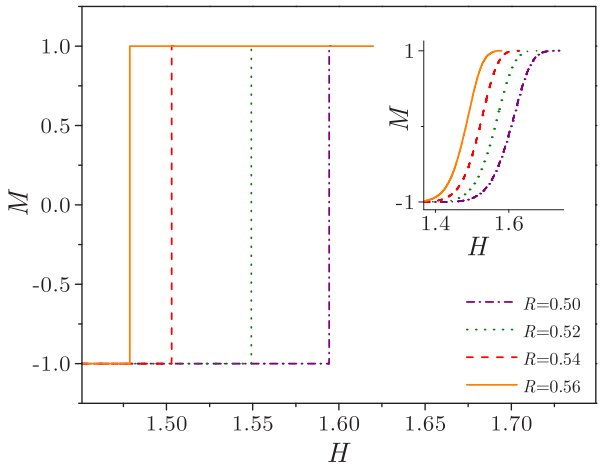

FIG. 23. (Color online) Magnetization curves $M(H)$ for disorders $R = 0.50$–0.56 and lattice size $L = 2896$; the effective critical disorder for this size of 2D lattice is $R_c^{\rm eff} = 0.701$. Main panel: magnetization curves for single random field configurations. Inset: Magnetization curves averaged over 40 000 random field configurations.

where $M_s(H;R,L)$ comes from spanning avalanches, and $M_{ns}(H;R,L)$ from nonspanning avalanches. The contribution from nonspanning avalanches scales as

$$M_{ns}(H;R,L) = L^{-\beta/\nu}\mathcal{M}_{ns}(h'L^{\beta\delta/\nu},|r|L^{1/\nu}), \tag{43}$$

where β, δ, and ν are the (standard) critical exponents of the 2D model, and $\mathcal{M}_{ns}(h'L^{\beta\delta/\nu},|r|L^{1/\nu})$ is the corresponding universal scaling function.

Above $R_c^{\rm eff}(L)$, the spanning avalanche contribution $M_s(H;R,L) = 0$, because the spanning avalanches are absent. In this case, the averaged magnetization $M(H;R,L)$ coincides with the nonspanning avalanche part $M_{ns}(H;R,L)$, and scaling (43) corresponds to scaling (1) in Ref. [11].

Below $R_c^{\rm eff}(L)$, the part of change of averaged magnetization, caused by the spanning avalanches triggered in the infinitesimal interval dH around the external field H, is given by

$$dM_s(H;R,L) = \frac{2}{L^2}\sum_\alpha \langle S\rangle_{\alpha|H;R,L} N'_\alpha(H;R,L)dH, \tag{44}$$

where $\langle S\rangle_{\alpha|H;R,L}$ is the *conditional* average size of α-type of spanning avalanches that are, for given disorder R and lattice size L, triggered in that interval dH of the external magnetic field. Our data show that for each type of spanning avalanches the conditional average size $\langle S\rangle_{\alpha|H;R,L}$ is practically *constant* in the entire range of the spanning field, i.e.,

$$\langle S\rangle_{\alpha|H;R,L} \simeq \langle S\rangle_\alpha, \tag{45}$$

where $\langle S\rangle_\alpha$ is the (usual) average size, introduced in Sec. VI. Therefore, for $M_s(H;R,L) = \int dM_s(H;R,L)$, we find that

$$M_s(H;R,L) = \frac{2}{L^2}\sum_\alpha \langle S\rangle_\alpha N^*_\alpha(H;R,L), \tag{46}$$

where

$$N^*_\alpha(H;R,L) \equiv \int_{H_c+b(R-R_c)/R}^{H} N'_\alpha(\tilde H;R,L)d\tilde H, \tag{47}$$

or in alternative notation

$$N^*_\alpha(h';r,1/L) = \int_0^{h'} N'_\alpha(\tilde h';r,1/L)d\tilde h' \equiv N^*_\alpha(H;R,L); \tag{48}$$

see Ref. [26]. For $h' > 0$, $N^*_\alpha(h';r,1/L)$ equals the average number per single run of α-type of spanning avalanches, triggered in the interval $[0,h']$ of reduced magnetic field, and for $h' < 0$, the negative of the number of these avalanches, triggered in $[h',0]$.

The number of 1D-spanning avalanches $N_1^*(H;R,L)$ scales as

$$N_1^*(H;R,L) = L^{-\theta_1}\widetilde N_1^*(h'L^{\zeta_1},rL^{1/\nu}), \tag{49}$$

which follows from (32) and (48), and where $\widetilde N_1^*(h'L^{\zeta_1},rL^{1/\nu})$ is the universal scaling function. In regard to the quantities pertaining to 2D-spanning avalanches, the scaling of $N^*_{2-}(H;R,L)$ is of the same type as the scaling of $N^*_{2c}(H;R,L)$, namely,

$$N^*_{2-}(H;R,L) = \widetilde N^*_{2-}(h'/L^{\zeta_2},rL^{1/\nu}), \tag{50}$$

$$N^*_{2c}(H;R,L) = \widetilde N^*_{2c}(h'/L^{\zeta_2},rL^{1/\nu}), \tag{51}$$

with an analogous meaning of involved quantities.

The foregoing findings, together with the scaling prediction (23), enable us to propose the following expression for averaged magnetization:

$$\begin{aligned} M(H,R,L) = {} & L^{-\beta/\nu}\mathcal{M}_{ns}(h'L^{\beta\delta/\nu},rL^{1/\nu}) \\ & + \frac{2}{L^2}\Big[L^{d_f^{(2-)}}\Psi_{2-}(rL^{1/\nu})N^*_{2-}(h'/L^{\zeta_2},rL^{1/\nu}) \\ & + L^{d_f^{(2c)}}\Psi_{2c}(rL^{1/\nu})N^*_{2c}(h'/L^{\zeta_2},rL^{1/\nu}) \\ & + L^{d_f^{(1)}-\theta_1}\Psi_1(rL^{1/\nu})N_1^*(h'L^{\zeta_1},rL^{1/\nu})\Big]. \end{aligned} \tag{52}$$

Equation (52) shows that averaged magnetization $M(H;R,L)$ exhibits a mixed type of scaling that prevents exact collapsing of averaged magnetization curves below effective critical disorder. For large L, however, the middle part of the averaged magnetization curves can be approximately specified as

$$M(H,R,L) \approx 2\Psi_{2-}(rL^{1/\nu})N^*_{2-}(h'/L^{\zeta_2},rL^{1/\nu}), \tag{53}$$

because all other contributions are small due to

$$-\beta/\nu < d_f^{(1)} - \theta_1 < d_f^{(2c)} < 2 = d_f^{(2-)}.$$

In Fig. 24 we demonstrate that averaged magnetization curves, satisfying condition $rL^{1/\nu} = \text{const}$, collapse onto a single curve, after scaling along the horizontal axis according to prediction (53).

IX. DISCUSSION

Beside the many similarities, one has to notice some important differences between the spanning avalanches in the

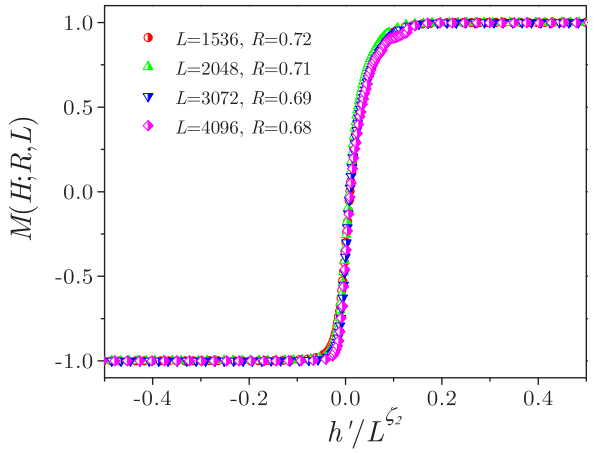

FIG. 24. (Color online) Collapse of averaged magnetization curves scaled according to Eq. (53); $\zeta_2 = -0.30$. The curves correspond to (L, R) pairs shown in the legend, satisfying condition $rL^{1/\nu} \approx$ const.

2D and the 3D case, which can be attributed to different topological properties of the underlying 2D and 3D lattices.

The most important difference, already discussed in Sec. III, is that there can be at most one spanning avalanche per single run in the 2D model, whereas in higher dimensions the spanning avalanches may be interlaced.

Next, the subcritical 2D-spanning avalanches play a more pronounced role in the 2D model than the analogous subcritical 3D-spanning avalanches in the 3D case. Indeed, below and at the critical disorder, the subcritical 2D-spanning avalanches dominantly influence analyzed intensive system characteristics (average number of spanning avalanches, moments of avalanche distributions, magnetization jumps, and averaged magnetization), whereas the contributions of other types of avalanches remain either small or vanish with the increase of system size, and this, in turn, makes the scaling analyses of large systems in the 2D model simpler then the corresponding analyses in the 3D case.

Additional dissimilarity between the 2D and the 3D model is related to the optimal choice of order parameter. Scaling analyses in the 3D model [21] are performed with the aid of order parameter u with tunable free parameter A [see Eq. (6)], which can be, according to our findings, avoided in the 2D case using usual (and simpler) parameter r.

Finally, we mention that the double finite-size scaling method, used in Ref. [21] for separation between subcritical and critical 3D-spanning avalanches, is impossible to apply in the 2D case because the exponent pertaining to the average number of 2D-spanning avalanches is zero in the 2D model. For this reason we have introduced a simple criterion based on the appropriate choice of $d_f^{(s)}$, the value of fractal dimension employed for separation of 2D-spanning avalanches into critical ($d_f < d_f^{(s)}$) and subcritical ($d_f \geqslant d_f^{(s)}$). The method is crude because of some uncertainty associated with the choice of $d_f^{(s)}$ [see Fig. 10], so it can obviously give a wrong classification in some individual cases. Although one may argue that it can be improved, or replaced by a better method, we believe that on average it works reasonably well, which is evidenced in our results.

X. CONCLUSION

In this paper we have presented an analysis of spanning avalanches in the two-dimensional nonequilibrium zero-temperature random field Ising model. The data were collected in extensive simulations of systems with linear sizes up to $L = 2^{15} = 16\,384$. Unlike in higher dimensions, the 2D predictions are obtained with the aid of reduced disorder-order parameter free of tunable coefficients.

According to the number of spanned spatial dimensions, spanning avalanches are classified as 1D and 2D-spanning avalanches, and the 2D-spanning avalanches are further classified as subcritical and critical. Distinction between the subcritical and critical 2D-spanning avalanches is carried out by a simple method, based on the value of fractal dimension that separates two components of the fractal dimension distribution of 2D-spanning avalanches.

For each of the avalanche types, we have performed finite-size scaling analysis in the case of distribution of average number of avalanches per single run, avalanche size distribution, average avalanche size, and contribution of individual avalanche types to magnetization jump.

In addition to the foregoing analyses, we have introduced a scaling analysis of the spanning field (i.e., that is field triggering the spanning avalanche) and analysis of magnetization curves averaged over random field configurations, which we managed to collapse below critical disorder.

Our study revealed that subcritical 2D-spanning avalanches play a dominant role in behavior of the 2D model, below, and at the critical disorder. Other types of avalanches influence statistics of finite 2D systems, but when the system size grows, their contribution remains small or vanishes.

ACKNOWLEDGMENTS

This work was supported by the Serbian Ministry of Education and Science under project 171027. We are grateful to the Scientific Computing Laboratory of Institute of Physics in Belgrade for providing computer facilities.

[1] D. P. Belanger and T. Nattermann, in *Spin Glasses and Random Fields*, edited by A. P. Young (World Scientific, Singapore, 1998).

[2] J. P. Sethna, K. A. Dahmen, and O. Perković, in *The Science of Hysteresis*, edited by G. Bertotti and I. Mayergoyz (Academic Press, Amsterdam, 2006).

[3] J. P. Sethna, K. A. Dahmen, S. Kartha, J. A. Krumhansl, B. W. Roberts, and J. D. Shore, Phys. Rev. Lett. **70**, 3347 (1993).

[4] L. Laurson, G. Durin, and S. Zapperi, arXiv:1306.5990v1.

[5] G. Durin and S. Zapperi, in *The Science of Hysteresis*, edited by G. Bertotti and I. Mayergoyz (Academic Press, Amsterdam, 2006).

[6] D. Spasojević, S. Bukvić, S. Milošević, and H. E. Stanley, Phys. Rev. E **54**, 2531 (1996).
[7] K. A. Dahmen and J. P. Sethna, Phys. Rev. Lett. **71**, 3222 (1993); Phys. Rev. B **53**, 14872 (1996).
[8] O. Perković, K. A. Dahmen, and J. P. Sethna, Phys. Rev. Lett. **75**, 4528 (1995); Phys. Rev. B **59**, 6106 (1999).
[9] O. Perković, K. A. Dahmen, and J. P. Sethna, arXiv:cond-mat/9609072v1.
[10] D. Spasojević, S. Janićević, and M. Knežević, Europhys. Lett. **76**, 912 (2006).
[11] D. Spasojević, S. Janićević, and M. Knežević, Phys. Rev. Lett. **106**, 175701 (2011).
[12] D. Spasojević, S. Janićević, and M. Knežević, Phys. Rev. E **84**, 051119 (2011).
[13] A. Maritan, M. Cieplak, M. R. Swift, and J. R. Banavar, Phys. Rev. Lett. **72**, 946 (1994); C. Frontera and E. Vives, Phys. Rev. E **59**, R1295 (1999); **62**, 7470 (2000); A. K. Hartmann, Phys. Rev. B **65**, 174427 (2002); E. Vives, M. L. Rosinberg, and G. Tarjus, *ibid*. **71**, 134424 (2005); B. Ahrens and A. K. Hartmann, *ibid*. **83**, 014205 (2011).
[14] Y. Liu and K. A. Dahmen, Europhys. Lett. **86**, 56003 (2009); Phys. Rev. E **79**, 061124 (2009).
[15] M. Aizenman and J. Wehr, Phys. Rev. Lett. **62**, 2503 (1989); Commun. Math. Phys. **130**, 3 (1990).
[16] Y. J. Chen, S. Papanikolaou, J. P. Sethna, S. Zapperi, and G. Durin, Phys. Rev. E **84**, 061103 (2011).
[17] B. A. W. Brinkman and K. A. Dahmen, Phys. Rev. E **84**, 041129 (2011).
[18] M. LeBlanc, L. Angheluta, K. Dahmen, and N. Goldenfeld, Phys. Rev. Lett. **109**, 105702 (2012).
[19] M. LeBlanc, L. Angheluta, K. Dahmen, and N. Goldenfeld, Phys. Rev. E **87**, 022126 (2013).
[20] P. Ispanovity, L. Laurson, M. Zaiser, I. Groma, S. Zapperi, and M. Alava, arXiv:1307.3377.
[21] F. J. Pérez-Reche and E. Vives, Phys. Rev. B **67**, 134421 (2003); **70**, 214422 (2004).
[22] E. T. Seppälä, V. Petäjä, and M. J. Alava, Phys. Rev. E **58**, R5217 (1998).
[23] E. T. Seppälä and M. J. Alava, Phys. Rev. E **63**, 066109 (2001).
[24] L. S. Liebovitch and T. Toth, Phys. Lett. A **141**, 386 (1989).
[25] Both N_s and $\langle S\rangle_s$ depend on disorder R and lattice size L, so they should be precisely denoted by $N_{s|R,L}$ and $\langle S\rangle_{s|R,L}$, which we avoid for the sake of simplicity.
[26] Let us note that all quantities (e.g., M_s and N_α^*) that depend on H, R, and L can be alternatively taken as functions of h', r, and $1/L$. For simplicity, we indicate the current independent variables in the variable list, and keep the same notation of the quantity itself. Thus, for example, $M_s(H;R,L)$ and $M_s(h';r,1/L)$ are, in fact, the same quantity, spanning avalanche part of averaged magnetization, but taken as a function of two different sets of independent variables, $(H;R,L)$ and $(h';r,1/L)$, respectively.